Quantitative infrared imaging of silicon-on-insulator microring resonators

Michael L. Cooper,[1,*] Greeshma Gupta,[1] Jung S. Park,[1] Mark A. Schneider,[1] Ivan B. Divliansky,[2] and Shayan Mookherjea[1]

[1]*Department of Electrical and Computer Engineering, University of California, San Diego, 9500 Gilman Drive, MC 0407, La Jolla, California 92093-0407, USA*

[2]*CREOL, The College of Optics and Photonics, University of Central Florida, P.O. Box 162700, Orlando, Florida 32816-2700, USA*

**Corresponding author: mlcooper@ucsd.edu*

Received November 2, 2009; revised January 18, 2010; accepted January 22, 2010; posted February 2, 2010 (Doc. ID 119316); published February 26, 2010

There is considerable research activity in multiresonator optical circuits in silicon photonics, e.g., for higher-order filters, advanced modulation format coding/decoding, or coupled-resonator optical waveguide delay lines. In diagnostics of such structures, it is usually not possible to measure each individual microring resonator without adding separate input and output waveguides to each resonator. We demonstrate a noninvasive diagnostic method of quantitative IR imaging, applied here to a series cascade of rings. The IR images contain information on the otherwise inaccessible individual through ports and the resonators themselves, providing an efficient means to obtain coupling, loss, and intensity-enhancement parameters for the individual rings. © 2010 Optical Society of America

OCIS codes: 230.4555, 130.3120, 110.3080.

Silicon-on-insulator (SOI) integrated photonic circuits with one or several microring resonators are an active area of research. The particular multiring structure fabricated and tested here is a side-coupled integrated spaced sequence of resonators (SCISSOR), comprised of ten racetrack resonators as shown in Fig. 1. Such devices may be used for slow light [1] or as a linear or nonlinear self-limiting add–drop filter [2,3]. In recent years, IR imaging using vertically scattered light has been used for loss characterization of planar and SOI photonic crystal waveguides [4,5] and for the study of localization, polarization conversion, and dispersion in disordered waveguides [6–8]. Here we use IR imaging to simultaneously characterize several SOI microring resonators.

The device was fabricated on an SOI wafer with 250 nm silicon thickness and 3 μm buried oxide thickness, using electron-beam lithography and dry-etching. The ring and bus waveguides have a top layer of 200-nm-thick hydrogen silsequioxane, while air forms the side cladding. Using photolithography, 3 μm $\times$ 2 μm SU-8 couplers are patterned over 150-μm-long silicon waveguide inverse tapers. The ring radius is 25 μm, and the straight track length is 40 μm.

Structural imperfections during the fabrication can result in a variation in the microring resonant frequencies and coupling coefficients across the device. To study these variations, we propose and demonstrate a nondestructive method of investigating ring resonators and waveguides that can be scaled readily to handle much more complex optical circuits. Rayleigh scattering due to sidewall roughness is a source of radiative loss in high-index contrast SOI waveguides at telecommunication wavelengths. Some of this light can be collected by imaging the device plane onto a high-sensitivity IR camera through a microscope objective. This can be used to provide a local measure of the guided-light intensity, as the scattered light is directly proportional to the light-intensity guided in a waveguide or circulating within a resonator. Thus, using an IR camera to image the photonic circuit at multiple wavelengths and processing the resulting images can yield spectral intensity-enhancement and transmittance data.

Two light sources are used separately: a white-light source is used for broad-spectrum incoherent imaging of the chip, mainly for alignment purposes and determining averaging paths, as discussed later. Alternatively, TE-polarized coherent light from a tunable laser source is then coupled to the chip through a polarization-maintaining lens-tipped fiber, with 20 dB polarization extinction measured after the tip. An XEVA-FPA-1.7-320 12 bit IR camera (XenICs NV, Belgium, 320×256 pixel grid with a 30 μm pitch) is used to spatially image the chip through a 5$\times$ microscope objective lens. The maximum and minimum detectable powers per pixel (area = 36 μm^2), for a camera integration time of 4 ms, are 0.16 nW and 0.04 pW, respectively. Figure 1(b) shows a one-shot IR image of the entire SCISSOR device, when excited by a broadband source centered at a wavelength of 1570 nm. This image shows that for Rings 1–9 (starting at the top of the image), the end points of the drop waveguides, along the cleaved facet of the chip, scatter sufficient light. With this technique, the desired spectral content could also be tapped anywhere on the chip using grating couplers [9]. For the tenth ring, there was a fabrication defect that prevented the drop port from being measured accurately and, instead, the encircled defect at a point along the waveguide was used. In the close vicinity of these measurement sites, a spatial average of 4×4 pixel intensities is computed from an array of IR images obtained at each wavelength, during a 10 pm step scan of the tunable laser source. Fig-

 © 2010 Optical Society of America

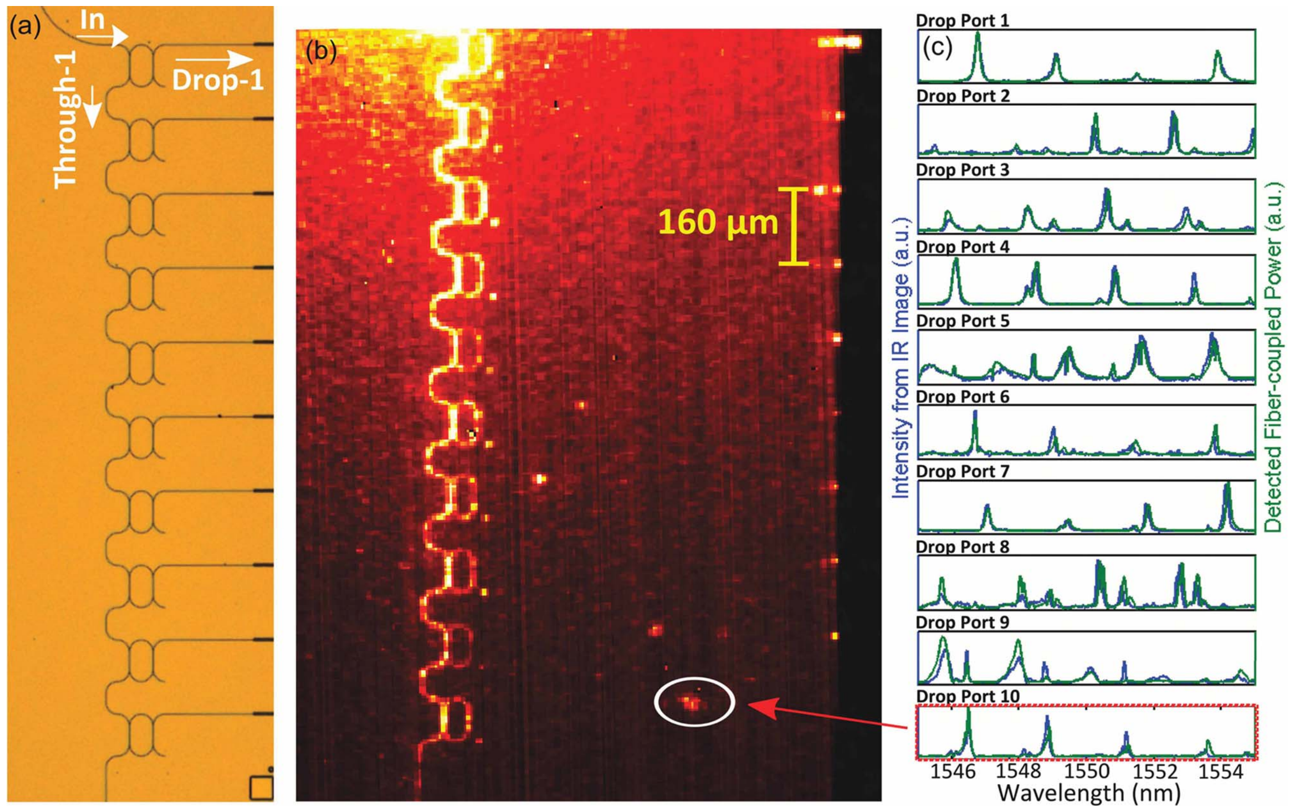

Fig. 1. (Color online) (a) Optical microscope image of ten-ring SCISSOR. (b) IR image of SCISSOR when excited by broadband source. (c) Using a tunable laser source, comparison of spectra obtained at the ten drop ports using IR images and spectra obtained from detected drop port power using fiber coupling. The spectrum for Ring 10 was obtained by measuring at the encircled waveguide defect.

ure 1(c) shows a comparison of the drop port transmission spectra obtained from imaging with the traditional method of measuring via a lensed fiber, translated (and realigned) sequentially from the first to the tenth drop port. Note that only a single alignment step (of the input) is necessary for the imaging approach, compared to 11 alignments (and ten tunable laser scans) for the lensed fiber approach. We observe very good agreement of data obtained from both methods.

IR imaging allows a non-invasive measurement of the through port transmittance of each ring within a multiring cascade, as would be necessary to determine the waveguide cross-coupling coefficient κ and the round-trip (amplitude) loss factor a [10,11]. Compared to slower serial-scan probing methods such as near-field scanning optical microscopy [12] and optical-fiber-based probes [13], IR imaging can measure several resonators simultaneously. The main disadvantage is the diffraction limited resolution.

Another set of images is obtained by scanning the tunable laser source wavelength and recording the IR images of Rings 1 and 2 at a higher magnification (20×). Figure 2(a) shows a typical IR imaging profile at a wavelength of 1533.90 nm. The waveguide profile is obtained by using an amplified spontaneous emission source to illuminate all ten rings. This profile is then converted to a binary matrix that is used to extract the desired paths which correspond to the input port, the through port, and the ring resonator. The pixel intensities are then averaged over these selected path lengths and normalized by the input to yield the spectra shown in Figs. 2(b) and 2(c). In order to compare different areas, the averaging regions should contain the same number of bends, junctions, or defects; otherwise, seemingly anomalous behavior can be observed for the magnitude of through port transmittance for Ring 1 (magnitude of the path-averaged output > path-averaged input). We emphasize that it is the ratios of the "on" and "off" resonance transmission values that are used to characterize the micro-rings [10,11].

The free spectral range (FSR), resonator bandwidth (BW), and normalized through port transmittance $T_{\min}$ are obtained from the through port transmission spectrum. For a Ring 1 resonance at $\lambda_{\text{res}} = 1530.45$ nm, FSR = 2.31 nm (296 GHz), BW = 0.12 nm (15 GHz), and $T_{\min} = 0.65$. Using the expressions in [10], the relevant ring parameters are extracted and summarized in Table 1. α_{RT} is the loss

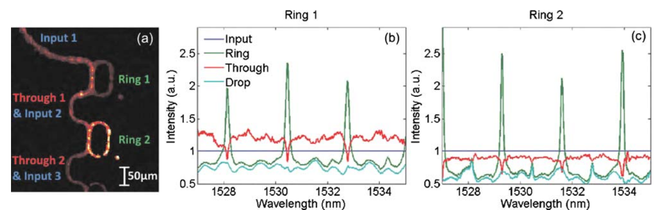

Fig. 2. (Color online) (a) IR image of Rings 1 and 2, at an input wavelength of 1533.90 nm, used toward obtaining spectra for through port, drop port, and circulating ("Ring") powers, normalized by the input, for Rings (b) 1 and (c) 2.

Table 1. Extracted Resonator Parameters

	Ring 1		Ring 2	
λ_{res} (nm)	1530.45	1532.77	1529.30	1531.60
κ^2	0.032	0.035	0.022	0.020
a	0.859	0.832	0.878	0.861
α_{RT} (dB)	1.32	1.60	1.13	1.30
I_{calc}	3.06	2.64	3.66	3.34
I_{meas}	2.36	2.08	2.50	2.11

(in decibels) per round trip in the ring. I_{calc} is the intensity-enhancement factor of the ring, calculated as the number of round trips N of a circulating photon, which is the ratio of the photon lifetime τ_{ph} and the time taken to complete one round trip of the ring, T_{RT},

$$N = \frac{\tau_{ph}}{T_{RT}} = \frac{Q/\omega_0}{1/\mathrm{FSR}_{freq}} = \frac{\mathrm{FSR}_{freq}}{\mathrm{BW}}\frac{1}{2\pi} = \frac{F}{2\pi}, \qquad (1)$$

where ω_0 is the radial resonance frequency and F is the finesse of the resonator. In Table 1, $I_{calc}=N$ is compared against I_{meas}, which is the peak circulating intensity at a resonant wavelength, read off from Figs. 2(b) and 2(c).

Scanning electron microscope (SEM) images convey a waveguide width of 540 nm and a resonator-waveguide gap of 310 nm. Using an effective coupler length [14] of 51 μm, we estimate κ^2 to be 0.036, which is close to the values extracted from the imaging data. The high loss is consistent with the $\geq$10 nm sidewall roughness [15] observed using the SEM. The corresponding intrinsic quality factor is 15,900, while the loaded Q is 12,750. For high-Q resonators, we expect the enhancement factor to compensate for low intrinsic scattering losses. For our ring structure, the enhancement factor will compensate for an intrinsic scattering loss as low as 0.001 dB/cm, which corresponds to an intrinsic Q-factor of 7.6×10^8.

In summary, IR imaging has been applied for the characterization of individual rings in a multi-ring structure toward understanding the overall device performance and the desired post-fabrication tuning. This technique is readily scalable to measure multiple devices using larger fields of view and cameras with an increased number of pixels. Whereas the individual drop ports are accessible in the SCISSOR structure considered here, they are not accessible in many other multiresonator structures such as the coupled-resonator optical waveguide [6], for which this measurement technique may prove especially useful.

The authors are grateful for support from the National Science Foundation (NSF) (ECCS-0642603 and ECCS-0723055) and the University of California (UC) Laboratory Research Program. J. S. Park acknowledges sponsorship support from the NSF Graduate Research Fellowship Program.

References

1. J. E. Heebner, P. Chak, S. Pereira, J. E. Sipe, and R. W. Boyd, J. Opt. Soc. Am. B **21**, 1818 (2004).
2. S. T. Chu, B. E. Little, W. Pan, T. Kaneko, S. Sato, and Y. Kokubun, IEEE Photon. Technol. Lett. **11**, 691 (1999).
3. S. Mookherjea and M. A. Schneider, Opt. Express **16**, 15130 (2008).
4. V. Aggarwal and S. Aditya, Proc. SPIE **4579**, 310 (2001).
5. S. J. McNab, N. Moll, and Y. A. Vlasov, Opt. Express **11**, 2927 (2003).
6. S. Mookherjea, J. S. Park, S. H. Yang, and P. R. Bandaru, Nat. Photonics **2**, 90 (2008).
7. J. Topolancik, F. Vollmer, R. IIic, and M. Crescimanno, Opt. Express **17**, 12470 (2009).
8. N. Le Thomas, V. Zabelin, R. Houdre, M. V. Kotlyar, and T. F. Krauss, Phys. Rev. B **78**, 125301 (2008).
9. G. Roelkens, D. V. Thourhout, and R. Baets, Opt. Lett. **32**, 1495 (2007).
10. S. Xiao, M. H. Khan, H. Shen, and M. Qi, Opt. Express **15**, 10553 (2007).
11. F. Xia, L. Sekaric, and Y. A. Vlasov, Opt. Express **14**, 3872 (2006).
12. G. H. Vander Rhodes, B. B. Goldberg, M. S. Unlu, S. T. Chu, and B. E. Little, IEEE J. Sel. Top. Quantum Electron. **6**, 46 (2000).
13. K. Srinivasan, P. E. Barclay, M. Borselli, and O. Painter, Phys. Rev. B **70**, 081306(R) (2004).
14. G. Gupta, Y. H. Kuo, H. Tazawa, W. H. Steier, A. Stapleton, and J. D. O'Brien, Appl. Opt. **48**, 5324 (2009).
15. F. Grillot, L. Vivien, S. Laval, D. Pascal, and E. Cassan, IEEE Photon. Technol. Lett. **16**, 1661 (2004).